Remote-Sensing Retrieval of Oceanic Inherent Optical Properties by Inversion of the Radiative Transfer Equation

Curtis D. Mobley
Lydia K. Sundman

Sequoia Scientific, Inc.
Westpark Technical Center
15317 NE 90th Street
Redmond, WA 98052

FINAL REPORT

Prepared for the
Office of Naval Research
under
Contract No. N00014-01-M-0268

July 2002

SEQUOIA

REPORT DOCUMENTATION PAGE

Form Approved
OMB No. 074-0188

1. AGENCY USE ONLY (Leave blank)	2. REPORT DATE	3. REPORT TYPE AND DATES COVERED
	July 2002	Final Report, Aug 2001 to July 2002

4. TITLE AND SUBTITLE
Remote-sensing retrieval of oceanic inherent optical properties by inversion of the radiative transfer equation

5. FUNDING NUMBERS
N00014-01-M-0268

6. AUTHOR(S)
Curtis D. Mobley
Lydia K. Sundman

7. PERFORMING ORGANIZATION NAME(S) AND ADDRESS(ES)
Sequoia Scientific, Inc.
15317 NE 90th St.
Redmond, WA 98052-3562

8. PERFORMING ORGANIZATION REPORT NUMBER
Final Report-Item 0004

9. SPONSORING / MONITORING AGENCY NAME(S) AND ADDRESS(ES)
Environmental Optics Program, Code 322OP
Office of Naval Research
800 North Quincy Street
Arlington, VA 22217-5000
Attn: Dr. Joan Cleveland

10. SPONSORING / MONITORING AGENCY REPORT NUMBER

11. SUPPLEMENTARY NOTES

12a. DISTRIBUTION / AVAILABILITY STATEMENT
Unlimited

12b. DISTRIBUTION CODE

13. ABSTRACT ***(Maximum 200 Words)***

A shape-factor formulation of the radiative transfer equation (RTE) is developed to yield exact expressions for the remote sensing reflectance, R_{rs}, and the equivalent remotely sensed reflectance, RSR_a. This form of the RTE is configured for inherent optical property (IOP) retrievals via standard linear matrix inversion methods. Our inversion algorithm for the shape-factor RTE is exact in the sense that no approximations are made to the RTE. Thus errors in retrieved inherent optical properties (IOPs) are produced only by uncertainties within (1) the models for the shape factors and related quantities and (2) the IOP models required for inversion. Hydrolight radiative transfer calculations are used to derive analytical models for the various shape factors and related quantities for Case 1 waters. These shape factor models can predict the shape factors with accuracies ranging typically from two to 20%. Using the modeled shape factors, we are able to predict the in-air remotely sensed reflectance RSR_a to within 20% of the correct (Hydrolight-computed) values 96% of the time for the synthetic data used to determine the shape factor models, and to predict RSR_a to within ± 0.0005 sr^{-1} 86% of the time.

14. SUBJECT TERMS
remote sensing, Hydrolight, radiative transfer inversion

15. NUMBER OF PAGES
32

16. PRICE CODE

17. SECURITY CLASSIFICATION OF REPORT	18. SECURITY CLASSIFICATION OF THIS PAGE	19. SECURITY CLASSIFICATION OF ABSTRACT	20. LIMITATION OF ABSTRACT
UNCLASSIFIED	UNCLASSIFIED	UNCLASSIFIED	Unlimited

Executive Summary

Given measured water-leaving radiances or remote-sensing reflectances, it is not possible to invert the radiative transfer equation (RTE) to obtain the water column absorption and backscatter coefficients unless additional assumptions are made, or additional information is added, to constrain the inversion. One approach to constraining the inversion is to model selected unknowns—the so called shape factors and related quantities—as well as possible in terms of known quantities, and then treat the shape factors as known in the inversion process. This reduces the number of unknowns in the inversion, at the expense of introducing uncertainties via the imperfectly modeled shape factors. Clearly, the ultimate success of the inversion then depends on how well the shape factors can be modeled. This paper presents preliminary models for several shape factors and related quantities that are needed in the inversion of the radiative transfer equation. The models presented here were developed using a data base of Hydrolight-generated synthetic data for homogeneous Case 1 waters whose inherent optical properties (IOPs) are described by simple bio-optical models for the absorption and scattering coefficients.

If IOPs such as the absorption and backscatter coefficients are recovered as part of an iterative inversion algorithm, then the recovered IOPs can be used to model the shape factors because both the recovered IOPs and the IOP-dependent shape factors are iteratively improved during the course of the RTE inversion. In the present modeling, we considered the absorption coefficient a, the beam attenuation coefficient c, and the backscatter coefficient b_b to be the recovered (i.e., known) IOPs. The newly developed IOP-dependent shape factor models can predict the shape factors with accuracies ranging typically from two to 20%. Using the modeled shape factors, we are able to predict the in-air remotely sensed reflectance (RSR, which is equivalent to the remote sensing reflectance R_{rs}) to within 20% of the correct (Hydrolight computed) values 96% of the time for the synthetic data used to determine the shape factor models, and to predict RSR to within ± 0.0005 sr^{-1} 86% of the time. These results are very encouraging and warrant the continued development of the RTE inversion algorithm and its evaluation using both synthetic (Hydrolight generated) data and real data obtained at sea.

The details of this work are presented here in a format suitable for submission to the *Journal of Geophysical Research* as the first part of a two-part paper. The present Part I presents the underlying theory and models for the shape factors and related quantities. Part II will present the results of the application of the RTE inversion algorithm to both synthetic and real data.

Inversion of the Radiative Transfer Equation via Shape Factor Models. Part I: Theory and Shape Factor Models

Curtis D. Mobley
Lydia K. Sundman
Sequoia Scientific, Inc.
Westpark Technical Center
15317 NE 90th Street
Redmond, WA 98052

Frank E. Hoge
National Aeronautics and Space Administration
Goddard Space Flight Center
Wallops Flight Facility
Wallops Island, Virginia 23337

Paul E. Lyon
E. G. & G. Inc.
Wallops Flight Facility
Wallops Island, Virginia 23337

Running head: RTE Inversion via Shape Factors

Key words: remote sensing, optical oceanography, inverse modeling, radiative transfer theory

For submission to *Journal of Geophysical Research–Oceans*

ABSTRACT

We first show that the in-water, shape-factor formulation of the radiative transfer equation (RTE) can be modified to yield exact in-air expressions for the remote sensing reflectance, R_{rs}, and the equivalent remotely sensed reflectance, RSR_a. Our form of the RTE can be configured for inherent optical property retrievals via standard linear matrix inversion methods. Linear matrix inversion of the shape-factor RTE is exact in the sense that no approximations are made to the RTE. Thus errors in retrieved inherent optical properties (IOPs) are produced only by uncertainties within (1) the models for the shape factors and related quantities and (2) the IOP models required for inversion. We then use Hydrolight radiative transfer calculations to derive analytical models for the backscattering shape factor, radiance shape factor, fractional forward scattering coefficient, ratio of air-to-water mean cosines, and diffuse attenuation coefficient for in-water upwelling radiance for Case 1 waters. These shape factor models can predict the various shape factors with accuracies ranging typically from two to 20%. Using the modeled shape factors, we are able to predict the in-air remotely sensed reflectance RSR_a to within 20% of the correct (Hydrolight-computed) values 96% of the time for the synthetic data used to determine the shape factor models, and to predict RSR_a to within ± 0.0005 sr^{-1} 86% of the time. Error propagation matrices suggest that inherent optical property retrievals are primarily influenced by uncertainties in the backscattering shape factor, rather than by uncertainties in the remaining shape factors and their related components. Our model for the backscattering shape factor gives predictions that are correct to within 5% for 96% of the synthetic data points used to develop the model.

1. Introduction

Semianalytic radiance models [Gordon et al., 1988; Morel and Gentili, 1996] can be readily inverted by linear matrix methods [Hoge et al., 1999a,b] to provide oceanic inherent optical properties (IOPs). Such inversions are well conditioned [Hoge and Lyon, 1996] and promise a powerful method of simultaneously retrieving constituent absorption and backscattering coefficients in the upper surface layer of the world's oceans using satellite data. However, semianalytic radiance models do not provide an exact framework to account for all possible environmental and viewing conditions [Weidemann et al., 1995].

The radiative transfer equation (RTE) can provide exact inverse solutions, but the RTE is not easily inverted for many remote sensing situations [Zaneveld, 1995]. We therefore investigate the inversion of a specific form of the RTE, namely a modified version of the shape-factor formulation of Zaneveld [1995]. Some of the motivation for this work comes from the distinct need for highly accurate methods to retrieve the absorption coefficients of the chlorophyll accessory pigment phycoerythrin [Hoge et al., 1999b]. To this end the absorption coefficients of chlorophyll and CDOM must be accurately retrieved, otherwise weaker absorbing constituents (such as phycoerythrin) will be obscured.

In this paper we (1) show that the shape-factor form of the RTE can be readily configured into linear form for simultaneous retrieval of oceanic IOPs using standard matrix methods; (2) derive the RTE inversion for the principal "big three" IOPs, namely the phytoplankton absorption coefficient, the CDOM+detritus absorption coefficient, and the total constituent backscattering coefficient; (3) develop shape factor and related models required for inversion, namely backscattering and radiance shape factors, the diffuse attenuation coefficient for upwelling radiance, the ratio of average cosines of the air and water downwelling irradiances, and the fractional forward scattering coefficient; and (4) assess the propagation of errors into the IOP state vector resulting from errors in the data-model matrix and hydrospheric vector as well as shape factor and related models. Our ultimate objective is to determine if the shape-factor RTE matrix inversion methodology will result in accurate and efficient algorithms for application to satellite ocean color data. The present paper presents the underlying theory and develops the needed models for the shape factors and related quantities. The companion paper [Hoge et al, 2002] applies this theory to synthetic and real data.

2. The Shape Factor Form of the Radiative Transfer Equation

In a plane parallel medium without internal sources or inelastic scattering, the radiative transfer equation is

$$\cos\theta \frac{dL(\theta,\varphi,z)}{dz} = -c(z)\, L(\theta,\varphi,z) + \int_0^{2\pi}\int_0^{\pi} \beta(\theta,\varphi;\theta',\varphi';z)\, L(\theta',\varphi',z) \sin\theta'\, d\theta'\, d\varphi' . \qquad (1)$$

(See Notation section for definition of symbols.) Zaneveld [1995, 1982] showed that the Eq. (1) can be rewritten in terms of the *in-water* remotely sensed reflectance (RSR) as

$$RSR = \frac{L_u(\theta,\varphi,z)}{E_{od}(z)} = \frac{f_b(\theta,\varphi,z)\ \dfrac{b_b(z)}{2\pi}}{-\cos\theta\, k(\theta,\varphi,z) + c(z) - f_L(\theta,\varphi,z)\, b_f(z)}, \qquad (2)$$

where the dimensionless *backscatter shape factor* $f_b(\theta,\varphi,z)$ is given by

$$f_b(\theta,\varphi,z) = \frac{\displaystyle\int_0^{2\pi}\int_0^{\pi/2} \beta(\theta,\varphi;\theta',\varphi',z)\, L_d(\theta',\varphi',z) \sin\theta'\, d\theta'\, d\varphi'}{\dfrac{b_b}{2\pi} E_{od}(z)}, \qquad (3)$$

the dimensionless *radiance shape factor* $f_L(\theta,\varphi,z)$ is given by

$$f_L(\theta,\varphi,z) = \frac{\displaystyle\int_{\pi/2}^{2\pi}\int_0^{\pi} \beta(\theta,\varphi;\theta',\varphi',z)\, L_u(\theta',\varphi',z) \sin\theta'\, d\theta'\, d\varphi'}{b_f(z)\, L_u^{\mathrm{iso}}(z)}, \qquad (4)$$

and the *diffuse attenuation function for upwelling radiance* $k(\theta,\varphi,z)$, with units of 1/meters, is given by

$$k(\theta,\varphi,z) = -\frac{1}{L_u(\theta,\varphi,z)} \frac{dL_u(\theta,\varphi,z)}{dz} . \qquad (5)$$

Equation (2) is Zaneveld's [1995] Eq. (7) and is exact because it is simply a restatement of the RTE (1) for upward directions using definitions (3)-(5). Subscripts d and u on the radiance L explicitly

remind us that the radiance in Eq. (3) is downwelling ($0 \le \theta \le \pi/2$), whereas the radiance in Eqs. (4) and (5) is upwelling ($\pi/2 < \theta \le \pi$).

The numerator of the f_b shape factor of Eq. (3) shows how much downwelling radiance is scattered upward into direction (θ,φ). The denominator is the same quantity evaluated for the special case of an isotropic volume scattering function (in which case $\beta = 2b_b/4\pi$). Thus the f_b shape factor is a measure of how much the actual phase function differs from a constant over the backscattering directions. Similarly, the numerator of f_L in Eq. (4) shows how much up the upwelling radiance is forward scattered into direction (θ,φ). The denominator is the same quantity evaluated for the special case of an isotropic upwelling radiance distribution whose magnitude is L_u^{iso}, and for the special case of an isotropic volume scattering function. Clearly, these shape factors depend both on the IOPs (namely on the volume scattering function, in this case) and on the ambient radiance distribution, as does the diffuse attenuation coefficient of Eq. (5). These quantities therefore are unknown terms in Eq. (2), if Eq. (2) is to be inverted to obtain the IOPs a and b_b from measured upwelling radiances and downwelling irradiances. The fact that shape factors are unknown prevents the RTE (2) from being inverted unless further assumptions are made about the values of the shape factors. Modeling these unknowns in terms of known quantities is the major focus of this paper.

Equations (1)-(5) are valid at any depth within an arbitrarily stratified water column. Our interest is in remote sensing of near-surface water IOPs. We therefore need to relate the quantities in Eqs. (2)-(5), when evaluated just beneath the mean sea surface, to quantities in air just above the sea surface, which can be deduced via in-air remote sensing techniques. Equation (2) can be converted into a form suitable for above-water remote sensing applications as follows. The n-squared law for radiance transmittance across a boundary between two media [Mobley, 1994, Eq. (4.21)] can be used to convert the in-water upwelling radiance just beneath the sea surface, $L_u(\theta,\varphi,z=0)$, to the water-leaving radiance just above the sea surface, $L_{ua}(\theta_a,\varphi)$:

$$L_u(\theta,\varphi,z=0) = \frac{n_w^2}{t} L_{ua}(\theta_a,\varphi) . \qquad (6)$$

Subscript a denotes values in air, just above the mean sea surface; depth $z = 0$ denotes values in water, just beneath the sea surface. The in-air polar angle θ_a associated with $L_{ua}(\theta_a,\varphi)$ is the refracted viewing angle above the sea surface obtained by applying Snell's Law to the in-water angle θ. The downwelling scalar irradiance $E_{od}(z)$ is converted to the downwelling plane irradiance $E_d(z)$ via the mean cosine of the downwelling radiance, $\bar{\mu}_d$: $E_{od}(z) = E_d(z)/\bar{\mu}_d$. The plane irradiance just beneath the sea surface can be related to the in-air value via [Mobley, 1994, Eq. (7.19)]

$E_d(z=0) = E_{da}\,\bar{t} / (1 + rR)$. Combining these results gives [Mobley, 1994, Eq. (10.27)]

$$\frac{L_u(\theta,\varphi,z=0)}{E_{od}(z=0)} = \frac{n_w^2\,(1-rR)\,\bar{\mu}_d}{t\,\bar{t}}\;\frac{L_{ua}(\theta_a,\varphi)}{E_{da}}. \tag{7}$$

In Eq. (7), define $M \equiv [(t\,\bar{t})/[(1- rR)n_w^2]$. For a wide range of sky and sea surface conditions and for viewing directions relevant to remote sensing, M lies in the range of 0.53 to 0.55 [Mobley, 1994; Hoge and Lyon, 1996; Hoge et al., 1999a,b; Morel and Gentili, 1996]. Thus M can be approximated as $M \approx 0.54$, with an error of less than two per cent. Using Eq. (7) and partitioning the beam attenuation coefficient as $c(z) = a(z) + b_f(z) + b_b(z)$, Eq. (2) becomes

$$\begin{aligned} R_{rs} &= \frac{L_{ua}(\theta_a,\varphi)}{E_{da}} \\ &= \frac{M\,f_b(\theta,\varphi,0)\;b_b(0)/[2\pi\;\bar{\mu}_d(0)]}{-k(\theta,\varphi,0)\cos\theta\;+\;b_f(0)[1-f_L(\theta,\varphi,0)]\;+\;a(0)\;+\;b_b(0)}. \end{aligned} \tag{8}$$

Except for the small error associated with the assumed value for M, Eq. (8) remains an exact RTE expression for the in-air remote sensing reflectance, R_{rs}, just above the sea surface. The remote-sensing reflectance is the quantity used as the basis for ocean color remote sensing by the SeaWiFS [O'Reilly et al, 1998] and PHILLS [Davis et al, 2002] systems. R_{rs} can be obtained from at-sensor radiances after atmospheric correction; for our purposes here it is therefore considered known. As noted by Zaneveld [1995], it is desirable to use RSR_a, the in-air value of RSR, rather than R_{rs} because the scalar irradiance E_{od} is less sensitive to solar zenith angle effects than is the plane irradiance E_d. We thus use $RSR_a = \bar{\mu}_{da}\,R_{rs}$ to rewrite Eq. (8) as

$$\begin{aligned} RSR_a &= \frac{L_{ua}(\theta_a,\varphi)}{E_{oda}} \\ &= \frac{M\,\dfrac{f_b(\theta,\varphi,0)}{2\pi}\,\dfrac{\bar{\mu}_{da}}{\bar{\mu}_d(0)}\;b_b(0)}{-k(\theta,\varphi,0)\cos\theta\;+\;b_f(0)[1-f_L(\theta,\varphi,0)]\;+\;a(0)\;+\;b_b(0)}. \end{aligned} \tag{9}$$

The simplicity of Zaneveld's [1995] original in-water RSR formulation remains in this equation for RSR_a, except for M and the $\bar{\mu}_{da}/\bar{\mu}_d$ ratio for the downwelling light field. As a practical matter, Eq. (8) is presently more easily applied to field data because the in-air downwelling plane irradiance is more generally available, but there are no instrumental barriers to using scalar irradiance as in Eq. (9).

To further simplify Eq. (9) for later use, define the first term in the denominator as

$$D_L(\theta,\varphi,0) = -k(\theta,\varphi,0)\cos\theta\,. \tag{10}$$

We call D_L the *radiance derivative* term because it is a measure of the depth rate of change of the upwelling radiance, as seen in Eq. (5). Define the second term in the denominator as

$$B_f(\theta,\varphi,0) \equiv b_f(0)\,[1 - f_L(\theta,\varphi,0)]\,. \tag{11}$$

The shape factor f_L varies from 0.963 to 1.152 for nadir viewing [Weidemann et al., 1995; Zaneveld 1995]; thus B_f ranges from $0.037b_f$ to $-0.152b_f$, which is a small fraction of the forward scattering coefficient b_f. We therefore call B_f the *fractional forward scattering coefficient.* Thus, b_f and f_L are found in a combination in which one (f_L) serves to reduce the size of the other (b_f). Finally, define the mean cosine ratio as

$$R_\mu = \frac{\bar{\mu}_{da}}{\bar{\mu}_d(0)}\,. \tag{12}$$

Using definitions (10)-(12), Eq. (9) becomes

$$RSR_a(\theta_a,\varphi) = \frac{L_{ua}(\theta_a,\varphi)}{E_{oda}} = \frac{M\,\dfrac{f_b(\theta,\varphi,0)}{2\pi}\,R_\mu\,b_b(0)}{D_L(\theta,\varphi,0) + B_f(\theta,\varphi,0) + a(0) + b_b(0)}\,. \tag{13}$$

Equations (8), (9), and (13) are each called the shape-factor form of the RTE; we shall work with Eq. (13). Our ultimate goal is to use Eq. (13) to relate the unknown absorption and backscatter coefficients just beneath the sea surface to the known remotely sensed reflectance and other known quantities. As noted above, $M \approx 0.54$. However, the four quantities f_b, R_μ, D_L, and B_f [or, equivalently, f_b, R_μ, k, and $b_f(1-f_L)$ as seen in Eq. (9); for brevity we refer to all of these quantities as shape factors] are unknown. The shape factors depend in complicated ways on the water-column IOPs, environmental conditions (sky radiance, sea state), and viewing geometry (sun zenith angle, viewing direction). In Section 4 we show how to model the shape factors, so that they too can be considered known in Eq. (13).

Note finally that if D_L and B_f are both zero, then both R_{rs} and RSR_a are proportional to $b_b/(a + b_b)$, which is a well known approximate functional form for the dependence of these reflectances on the absorption and backscatter coefficients.

3. Linear Form of the Radiative Transfer Equation and Its Inversion

The in-air RSR_a of Eq. (13) immediately yields the fundamental linear form of the RTE,

$$a(0) + b_b(0)\,V + D_L + B_f = 0\,, \tag{14}$$

where

$$V(\theta,\varphi,0) = 1 - \frac{M\,\dfrac{f_b(\theta,\varphi,0)}{2\pi}\,R_\mu}{\dfrac{L_{ua}(\theta_a,\varphi)}{E_{oda}}}\,. \tag{15}$$

V is called the *backscattering enhancement factor* because, in general, $|V| > 10$.

We next partition the total absorption coefficient into contributions by pure water, phytoplankton, and CDOM plus detritus. Similarly, the backscatter coefficient is written as the sum of contributions by pure sea water and by particulate matter. It is easy to show [Hoge and Lyon 1996; Hoge et al., 1999a ; Hoge et al., 1999b] that the equation describing the desired phytoplankton absorption coefficient a_{ph}, CDOM+detritus absorption coefficient a_d, and total constituent backscattering coefficient b_{bt} resulting from Eq. (14) is

$$a_{ph}(\lambda_i) + a_d(\lambda_i) + b_{bt}(\lambda_i)\,V = -a_w(\lambda_i) - b_{bw}(\lambda_i)\,V - D_L - B_f. \tag{16}$$

The wavelength dependency of the IOP's is now shown explicitly, while the depth and angular dependencies have been suppressed for clarity. Note that the observed water-leaving radiances L_{ua} occur on both sides of the equation (within V). The pure-water absorption a_w is known from Pope and Fry [1997], and the water backscattering coefficient b_{bw} is given by Smith and Baker [1981]. The right hand side of Eq. (16) is therefore known, given the shape factors and a measurement of $RSR_a(\lambda_i)$. This linear form of the RTE is still exact in the sense that no approximations have been made to the RTE, but clearly the IOP retrieval accuracy will be determined by the accuracy of the shape factor models.

Given the water-leaving radiance at three wavelengths, Eq. (16) still cannot be solved for the "big three" IOPs, $a_{ph}(\lambda_i)$, $a_d(\lambda_i)$ and $b_{bt}(\lambda_i)$, because each measurement of $RSR_a(\lambda_i)$ yields an equation with three unknown IOPs. However, it is easy to show that a consistent solution is available by introducing spectral models for $a_{ph}(\lambda_i)$, $a_d(\lambda_i)$ and $b_{bt}(\lambda_i)$ [Hoge and Lyon 1996; Hoge et al., 1999a, Hoge et al., 1999b]. Substitution of such spectral models for $a_{ph}(\lambda_i)$, $a_d(\lambda_i)$ and $b_{bt}(\lambda_i)$ into Eq. (16)

yields

$$a_{ph}(\lambda_g)\exp\left[-\frac{(\lambda_i-\lambda_g)^2}{2g^2}\right] + a_d(\lambda_d)\exp\left[-S(\lambda_i-\lambda_d)\right] + b_{bt}(\lambda_b)\left(\frac{\lambda_b}{\lambda_i}\right)^n V = -a_w(\lambda_i) - b_{bw}(\lambda_i)\,V - D_L - B_f. \quad (17)$$

Equation (17) now has only three unknowns, $a_{ph}(\lambda_g)$, $a_d(\lambda_d)$ and $b_{bt}(\lambda_b)$, so that the system is solvable given measurements of $RSR_a(\lambda_i)$ at three wavelengths. This linear form of the radiative transfer equation remains exact and precise but, again, the uncertainty in the retrieved IOPs is now additionally influenced by the uncertainty in the IOP models [Hoge et al., 1999a].

At their respective reference wavelengths λ_g, λ_d , λ_b, the IOPs $a_{ph}(\lambda_g)$, $a_d(\lambda_d)$ and $b_{bt}(\lambda_b)$ are linearly related to the column matrix, or vector, containing the hydrospheric constants (sea water absorption and backscattering), radiances, and the shape factors. [It is easy to see from Eq. (16) that it is in principle possible to concurrently solve for the radiance derivative term $D_L(\lambda_i)$ and/or for the fractional forward scattering coefficient, B_f, in addition to the IOPs, given measurements of $RSR_a(\lambda_i)$ at additional wavelengths. However, the IOP models then must be of sufficient accuracy at yet a fourth and/or fifth wavelength, and the required wavelength dependency of these models was not a focus of this study. Therefore, such retrievals are beyond the scope of this initial RTE inversion work.] Equation (17) is very similar to the one used to analyze the effect of radiance errors and model uncertainties upon IOPs [Hoge and Lyon, 1996], and to retrieve IOPs from airborne upwelling radiances [Hoge et al., 1999a, b] when retrieved by semianalytic radiance model inversion. Equation 17 can therefore be written in matrix form as

$$\boldsymbol{D}\,\boldsymbol{p} = \boldsymbol{h}. \quad (18)$$

Here the hydrospheric vector $\boldsymbol{h}$ is given by the right hand side of Eq. (17). The IOP state vector is $\boldsymbol{p} = [a_{ph}(\lambda_g), a_d(\lambda_d), b_{bt}(\lambda_b)]^T$, where T denotes the transpose, and $\boldsymbol{D}$ is the data-model matrix [Hoge and Lyon 1996; Hoge et al., 1999a, b], which also contains shape factors. The IOPs are immediately determined from $\boldsymbol{p} = \boldsymbol{D}^{-1}\,\boldsymbol{h}$. (A least squares solution, $\boldsymbol{p} = [\boldsymbol{D}^T\,\boldsymbol{D}]^{-1}\,\boldsymbol{D}^T\,\boldsymbol{h}$, can be used if the number of sensor bands exceeds the number of unknown IOPs.)

The uncertainties in the IOP state vector $\boldsymbol{p}$ can be analyzed in a manner similar to other linear inversions [Hoge and Lyon, 1996]. Since $\boldsymbol{p} = \boldsymbol{D}^{-1}\,\boldsymbol{h}$, both $\boldsymbol{D}$ and $\boldsymbol{h}$ determine $\boldsymbol{p}$ and the errors that propagate into $\boldsymbol{p}$. Because the backscattering shape factor f_b is always found within $\boldsymbol{D}$, f_b influences

the propagation of errors into the IOPs more so than do the remaining factors. The discussion of the uncertainties in the IOP state vector $\boldsymbol{p}$ caused by possible singularity of $\boldsymbol{D}^{-1}$ and by perturbations in $\boldsymbol{D}$ somewhat parallels a similar previous discussion [Hoge and Lyon 1996] and is therefore provided in Appendix A.

4. Models for Shape Factors and Related Quantities

Inversion of Eq. (17) using remotely sensed ocean color data requires knowing V, D_L, and B_f. These quantities in turn depend on the shape factors f_b and f_L, the diffuse attenuation coefficient k, and the mean cosine ratio R_μ, as defined above. For ease of comparison with previous work on shape factors [Weidemann et al., 1995] and to make the underlying physics as transparent as possible, we explicitly model f_b, f_L, k, and R_μ, rather than D_L, and B_f. For notational convenience, we let X_i, i = 1,2,3, and 4, denote f_b, f_L, k, and R_μ respectively.

Because shape factors, diffuse attenuation functions, and mean cosines all depend on the ambient radiance, they depend implicitly on the solar zenith angle and viewing direction, as well as on the IOPs. The solar angle and viewing direction are known in any particular remote sensing situation; these geometric quantities are thus available for modeling the X_i in terms of known quantities. However, the IOPs are unknown. If we restrict ourselves to an explicit inversion of the RTE to obtain the IOPs, we must exclude the IOPs from the models for the X_i. However, if we perform an implicit, or iterative, inversion of the RTE, we can include the retrieved IOPs in the X_i models, for the following reason. In an iterative inversion, we start with an initial guess for the X_i, derived either from models that do not include IOPs or from physical intuition. (For example, a reasonable initial guess for f_b would be one, the value corresponding to a constant phase function. Similarly, $f_L = 1$, $k = 0$, and $R_\mu = 1$ would be acceptable initial guesses.) Using the initial guesses for the X_i, the RTE is inverted to obtain initial values for $a_{ph}(\lambda_g)$, $a_d(\lambda_d)$, and $b_{bt}(\lambda_b)$, from which the IOPs $a = a_t + a_w = a_{ph} + a_d + a_w$ and $b_b = b_{bt} + b_{bw}$ can be obtained at all wavelengths via the IOP models seen in Eq. (17). The X_i models developed below are based on an assumed phase function for particle scattering. Taking the particle phase function as known, the total constituent (particle) backscatter fraction $B_t = b_{bt}/b_t$ is also known. Thus the total constituent forward scatter coefficient b_{ft} can be obtained from the recovered b_{bt} and B_t: $b_{ft} = b_{bt}(1 - B_t)$. The total beam attenuation coefficient is then known from $c = a + b_{ft} + b_{bt} + b_w$. We therefore allow ourselves to develop models for the X_i that depend both on the known geometrical (viewing direction, solar direction) and physical (wind speed, wavelength) parameters, as well as on certain IOPs (namely a, c, and b_b).

4.1. The Database

To begin our analysis, 120 Hydrolight [Mobley and Sundman, 2001a, b] runs were made using its IOP model for Case 1 waters and the Petzold "average particle" phase function [Mobley et al., 1993] for scattering by the particles. This Case 1 IOP model is a two-component model: pure water plus "everything else." The non-water absorption and scattering coefficients are parameterized in terms of the chlorophyll concentration according to commonly used models seen in Mobley [1994, Eqs. (3.27) and (3.40).] The input for these runs covered a wide range of chlorophyll concentrations, solar zenith angles, cloud covers, and wind speeds. Each Hydrolight run generated output at various wavelengths, depths, and viewing directions. The resulting database potentially contains millions of records, where one record corresponds to a particular set of input values, output values for a particular viewing geometry, wavelength, depth, etc., and the values of the four X_i. Some of these records are not of great interest, e.g. records whose azimuthal viewing directions φ_v differ by only 15 degrees (the resolution of φ_v in the standard version of Hydrolight). Therefore, selected records were used to generate a database of more manageable size, but one that still covers the range of parameter values relevant to most remote sensing. Table 1 shows the input and output values in this database, which was used in the initial investigation of the functional forms of the X_i. Each of the four X_i was computed for each parameter combination represented in Table 1.

parameter	**values used in Hydrolight runs**
chlorophyll concentration, *Chl*	**0.1, 0.5, 1.0, 5.0, 10.0** mg m^{-3}
solar zenith angle, θ_s	**0.0, 10, 20, 30, 40, 60** degrees
wind speed	**0**, 10 m s^{-1}
cloud cover	**0**, 100%, i.e., clear sky and solid overcast
wavelength, λ	**412, 426, 440, 465, 490, 522.5, 555, 612, 670, 685** nm
polar viewing angle θ_v (in water, relative to the zenith)	**0.0, 10, 20, 30, 40**, 50, 60 degrees
azimuthal viewing angle φ_v (relative to sun)	0, **90**, 180 degrees
depth, *z*	**0**, 0.5, 1, 1.5, 2, 2.5, 3, 3.5, 4, 4.5, 5 m

Table 1. Parameters and their values used to generate the original database of 184,800 records. The values shown in bold correspond to the 1,500 records in the remote-sensing database.

We first examined the sensitivity of the X_i to the various parameters (wind speed, viewing direction, IOPs, etc) available for construction of models for the X_i. We found that the surface wind speed has a negligible effect on each of the X_i (less than one percent difference in X_i for the 0 and 10 m s^{-1} wind speeds, with all else being equal). This means that we could eliminate the wind speed from consideration in the subsequent modeling. Likewise, we considered only the clear-sky data, which are of greatest interest for remote-sensing applications. As noted above, for remote sensing applications we need to evaluate the shape factors X_i only at depth $z = 0$. (Note, however, that the values of the X_i at $z = 0$ incorporate the effects of all the absorption and multiple scattering occurring throughout the entire water column.) Thus we need retain only the output from the Hydrolight runs at $z = 0$. The original database included records generated for azimuthal viewing angles of $\varphi_v = 0$ (looking toward the sun) and $\varphi_v = 180$ degrees (looking away from the sun). Most remote sensing is done at azimuthal angles of $\varphi_v \approx 90$ degrees, which minimizes sun glint and instrument self-shading. Thus we retained only the records corresponding to $\varphi_v = 90$ degrees. Likewise, remote sensing generally uses in-air nadir viewing directions θ_{va} of less than 60 degrees, which corresponds to in-water angles $\theta_v \le 40$ degrees. Eliminating the larger in-water nadir viewing angles ($\theta_v = 50$ and 60 degrees in Table 1) gives a final "remote sensing" data set of 1500 records, which was used to determine models for the X_i. The parameter values corresponding to this remote-sensing database are shown in bold in Table 1.

4.2. Determining Functional Forms

Let P_k, $k = 1,...,N_k$, denote the parameters (wavelength, viewing direction, IOPs, etc) to be used in modeling the X_i. These parameters include those seen in Table 1, as well as the absorption, scattering, and backscattering coefficients (which are functions of the chlorophyll concentration if Case 1 water is assumed).

The simplest possible model for the X_i is a linear function of the P_k:

$$X_i = \sum_{k=1}^{N_k} \alpha_{ik} P_k , \quad i = 1,...,4 . \tag{19}$$

The α_{ik} are fitting coefficients whose values are to be determined; a different set of coefficients is needed for each factor X_i. We first set up a large linear least squares problem to see if this model was adequate to fit the various factors. Not surprisingly, the fits were unsatisfactory. In other words, the world is more complicated than Eq. (19).

The goal then became to develop models which could be nonlinear in the parameters, but which still reflect the underlying physics of the X_i. Thus we replace Eq. (19) by

$$X_i = \sum_{k=1}^{N(i)} F_{ik}(\{P_k\},\{\alpha_{ik}\}) . \tag{20}$$

This notation means that each function F_{ik} will contain some subset of the parameters P_k and will have its own set of fitting coefficients. For example, as we shall see in the next section, the model for f_b will contain terms involving the scattering-to-backscattering ratio and a nonlinear function of the three geometric parameters $(\theta_s,\theta_v,\varphi_v)$, with four fitting coefficients in all.

4.3. The Model for f_b

We now outline the development of the model for f_b. To obtain initial guidance about the possible functional form for an f_b model, we first used single-scattering theory to evaluate the definition of f_b seen in Eq. (3). According to the single scattering approximation (SSA), the downwelling radiance is [Gordon, 1994, Eq. (1.30)]

$$L_d(\theta',\varphi',z) = E_{od}\,\delta(\mu' - \mu_s)\,\delta(\varphi' - \varphi_s)\,e^{-cz/\mu_s} , \tag{21}$$

where $\mu = \cos\theta$ and (μ_s, φ_s) denotes the in-water direction of the sun's direct beam as refracted through a level sea surface; δ is the Dirac delta function. Inserting (21) into (3), integrating, and evaluating the result at $z = 0$, gives

$$f_b \approx 2\pi \frac{b}{b_b} \tilde{\beta}(\mu_s,\varphi_s,\mu,\varphi) . \tag{22}$$

Note that for isotropic scattering, $\tilde{\beta} = 1/4\pi$, $b = 2b_b$, and $f_b = 1$, as expected. As the phase function becomes more anisotropic, b/b_b increases, and f_b increases. In Eq. (22), the phase function tells us that, to first order, f_b involves downwelling radiance that is singly scattered from the sun's direct beam into the viewing direction. In remote sensing applications, the total phase function (water plus particles) will be unknown, but for any given phase function the contribution to f_b will depend on the scattering angle ψ corresponding to the sun's downward beam being scattered into the upward viewing direction. This scattering angle is equivalent to the easily computed sun-sensor included angle ξ, as shown in Fig. 1. Given the sun's location (θ_s, $\varphi_s = 0$) and the viewing direction (θ_v, φ_v), ξ is given by

$$\cos\xi = \cos\theta_s \cos\theta_v + \sin\theta_s \sin\theta_v \cos(\varphi_v) .$$

Thus, as a preliminary functional form for the f_b model, we consider

$$\hat{f}_b \propto \frac{b}{b_b} \Xi(\xi) ,$$

where $\Xi(\xi)$ is a function of angle ξ whose form is to be determined.

Figure 2 shows the 1,500 values of f_b in the remote sensing database plotted as a function of ξ and b/b_b. This figure suggests that a cosine function may capture the ξ dependence. Thus we try a model of the form

$$\hat{f}_b = \alpha_1 + \alpha_2 \frac{b}{b_b} \cos(\alpha_3 \xi) , \tag{23}$$

where α_1, α_2, and α_3 are fitting coefficients (the α_{ik} of Eq. (20) for model i =1) whose values are to be determined by minimizing the squared difference between $\hat{f}_b$ and f_b for the 1,500 values in the remote-sensing database. We do note from the color-coded points in Fig. 2 that f_b is largest for small b/b_b, and vice versa, which is contrary to the behavior predicted by Eq. (22). This reversal may be due to the dominance of multiple scattering in ocean waters, but further investigations would be necessary to understand this discrepancy between the SSA predictions and the Hydrolight predictions, which include all orders of multiple scattering and other effects not included in the SSA. In any case, there is a clear dependence on b/b_b, which can be modeled.

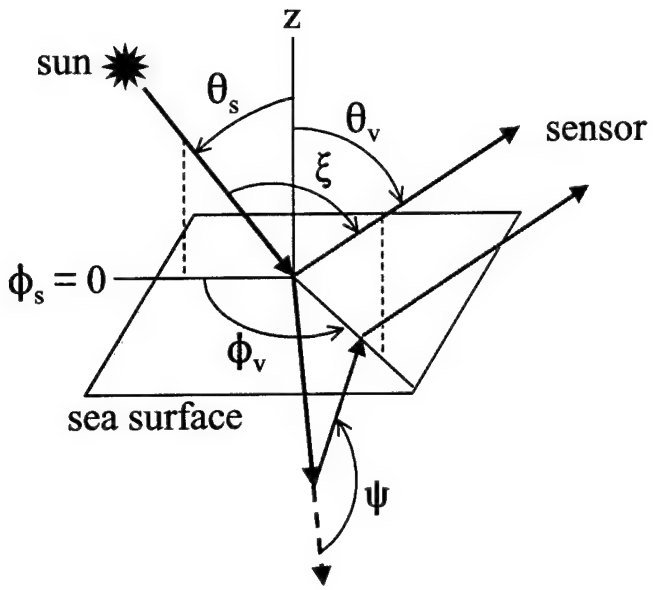

Fig. 1. Sun, sensor, and single-scattering geometry. The sea surface is shown in blue. The unscattered solar beam is in red, and the singly-scattered solar beam is in green.

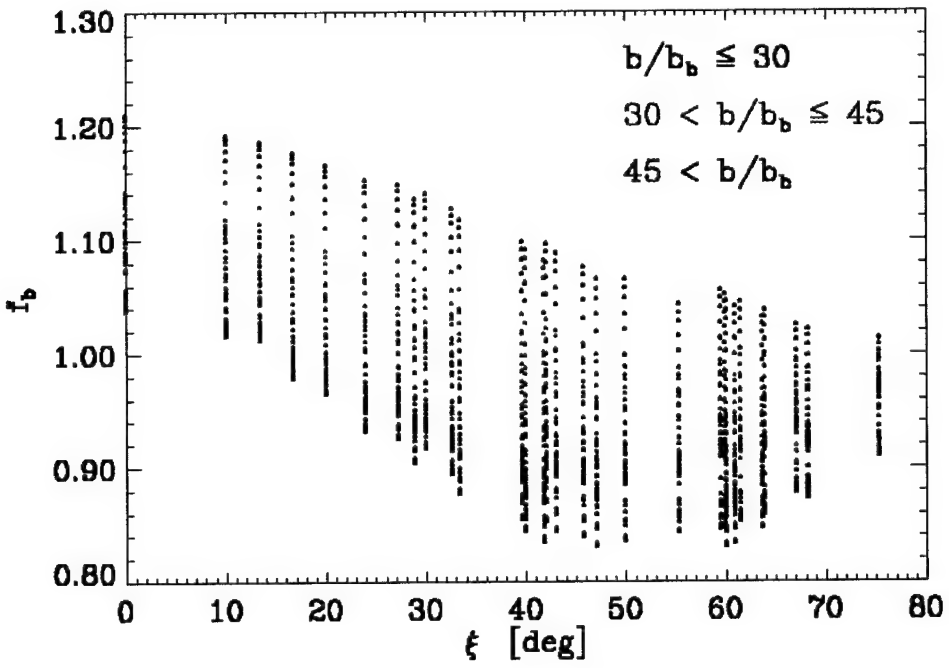

Fig 2. Values of f_b plotted as a function of sun-sensor included angle ξ and color coded to show the dependence on b/b_b.

The best-fit coefficients α_j in Eq. (23) were determined by least-squares minimization using a variety of numerical techniques appropriate for non-linear functions. After comparing the model predictions $\hat{f}_b$ with the actual f_b values, is was seen that not all of the b/b_b dependence was captured by the model of Eq. (23). Some experimentation showed that the remaining b/b_b dependence could be accounted for by adding another term proportional to b/b_b. Thus the final f_b took the form

$$\begin{aligned} \hat{f}_b &= \alpha_1 + \alpha_2 \frac{b}{b_b} \cos(\alpha_3 \xi) + \alpha_4 \frac{b}{b_b} \\ &= \alpha_1 + \alpha_4 \frac{b}{b_b} \left[1 + \frac{\alpha_2}{\alpha_4} \cos(\alpha_3 \xi) \right]. \end{aligned} \tag{24}$$

The second form of Eq. (24) shows that the additive term is equivalent to keeping the general form of the model suggested by the SSA, but picking a different angular function $\Xi(\xi)$. The complicated dependence of f_b on b/b_b and ξ is not surprising if one remembers that the $\Xi(\xi)$ function is fundamentally an attempt to parameterize the unknown phase function effects for a given sun and viewing geometry; thus the scattering and geometric effects are not independent. The final set of fitting coefficients for model (24) is shown in Table 2.

coefficient	**value**
α_1	1.2077
α_2	0.001977
α_3	3.3790
α_4	-0.004863

Table 2. Best-fit coefficients for the f_b model of Eq. (24).

Figure 3 shows the model and actual f_b values. The dashed lines are the 5% error bounds. Using the model of Eq. (24), 96.3% of the predicted values are within 5% of the correct value; the linear correlation coefficient between the model and actual points is $r = 0.955$. There is no systematic dependence on b/b_b or ξ of the model discrepancies seen in the individual points of Fig. 3. It would be possible to continue adding ad hoc terms in other variables to Eq. (24), and perhaps reduce the model-data discrepancy even more. However, such a process is likely to deviate from physical foundations, with the end result that the final model would not be applicable beyond the exact conditions used to generate the present remote-sensing data set. For this initial study, it is best to be content with the simple model of Eq. (24).

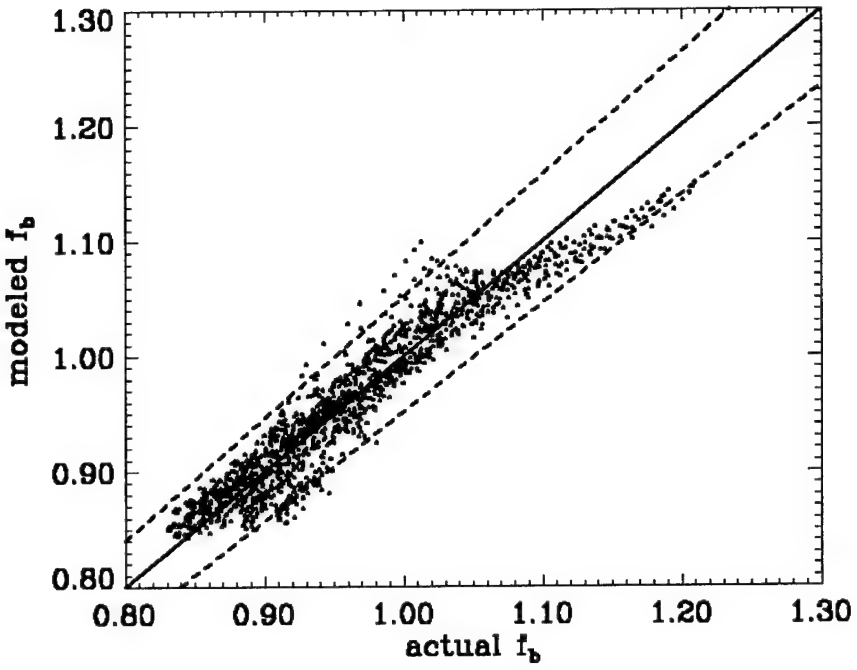

Fig. 3. Comparison of modeled and actual f_b values, using the model of Eq. (24). 96.3% of the modeled values lie within the dashed lines, which represent values with 5% of the correct value; the model-actual correlation coefficient is $r = 0.955$.

4.4. The Model for f_L

Just as with f_b, we first tried to use the SSA for guidance as to the general form of the model for f_L. In the SSA, the upwelling radiance is [Gordon, 1994, Eq. (1.32)]

$$L_u(\mu',\varphi',z) = \frac{b}{c} E_d(0)\, \tilde{\beta}(\mu_s,\varphi_s,\mu',\varphi') \frac{1}{\mu_s - \mu'} e^{-cz/\mu_s}. \tag{25}$$

Note that $\mu_s > 0$ and $\mu' < 0$. Inserting this SSA radiance into Eq. (4), the definition of f_L, integrating, and setting $z = 0$ gives

$$f_L \approx \frac{b^2 E_d(0)}{b_f c L_u^{iso}} \int_0^{2\pi} \int_0^{-1} \tilde{\beta}(\mu',\varphi',\mu,\varphi)\, \tilde{\beta}(\mu_s,\varphi_s,\mu',\varphi') \frac{1}{\mu_s - \mu'} d\mu'\, d\varphi'.$$

In most ocean waters, $b \approx b_f$. However, further simplification is difficult. The remaining integrals describe how the sun's downwelling direct beam is first scattered upward, and then scattered again into the viewing direction. The most we can say is that this is some function of the scattering phase function and the viewing geometry. As with f_b, we tried to parameterize this function in terms of the sun-sensor included angle ξ via a model of the form

$$\hat{f}_L \propto \frac{b}{c}\Xi(\xi).$$

Unfortunately, plots of f_L similar to Fig. 2 did not suggest a clear functional form for $\Xi(\xi)$ or show any significant dependence on b/c. This failure of the SSA to provide a functional form for f_L is not surprising because f_L inherently involves at least two scatterings, and multiple scattering can be expected to make an important contribution to the upwelling radiance.

We next examined the linear correlations between f_L and the various available fitting parameters. The results are seen in Table 3.

parameter	**correlation coef. r with f_L**
absorption coefficient a	0.291
scattering coefficient b	0.205
albedo of single scattering b/c	-0.076
backscatter coef b_b	0.180
forward scatter coef b_f	0.206
backscatter fraction b_b/b	-0.343
forward scattering fraction b_f/b	0.343
backscatter to absorption b_b/a	-0.231
wavelength λ	0.210
solar zenith angle θ_s	0.778
polar viewing angle θ_v	-0.006
sun-sensor included angle ξ	-0.562

Table 3. Correlation between the radiance shape factor f_L and various parameters.

The only potential model parameter that correlates even moderately strongly with f_L is the solar zenith angle θ_s. A plot of f_L vs. θ_s suggested a sine function for θ_s (although a simple linear function is almost as good). Thus we first tried a model of the form $\hat{f}_L = \alpha_1 + \alpha_2 \sin(\alpha_3 \theta_s)$. The residuals of this model showed a weak wavelength dependence. After considerable experimentation, we settled on the model

$$\hat{f}_L = \alpha_1 + \alpha_2 \left(\frac{\lambda}{550} \right) \sin(\alpha_3 \theta_s) . \tag{26}$$

The best-fit values of the coefficients are $\alpha_1 = 1.0247$, $\alpha_2 = 0.4584$ (for λ in nanometers), and $\alpha_3 = 0.1221$ (for θ_s measured in radians). Figure 4 shows the scatter plot for this model. 93.0% of the model predictions are within 2% of correct (points lying between the dashed lines); the correlation coefficient is $r = 0.829$. Although it is possible to obtain slightly better fits by including IOPs in an ad hoc fashion, we choose to stop with the model of Eq. (26) because of its simplicity and because of the lack of physical guidance for the IOP dependence.

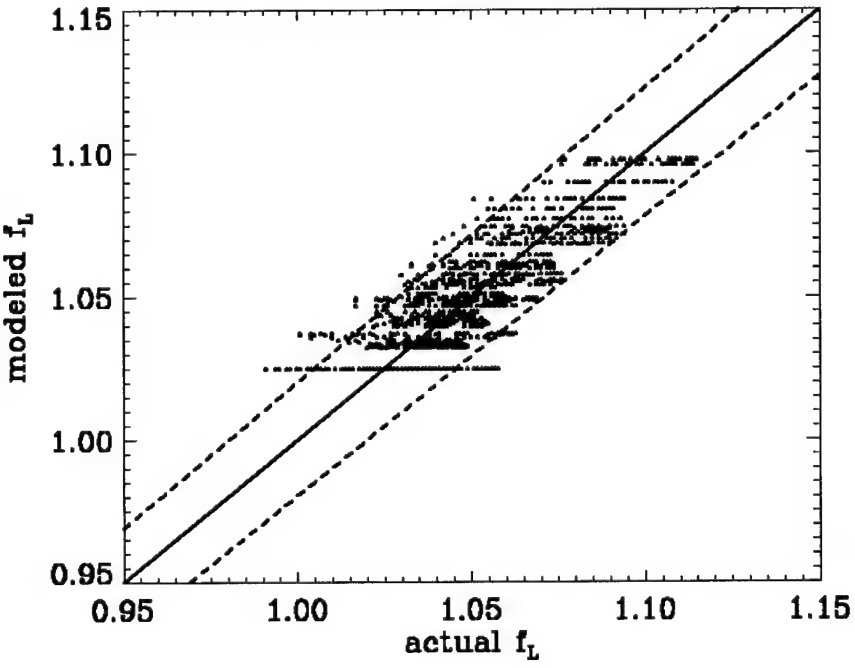

Fig. 4. Comparison of modeled and actual f_L values, using the model of Eq. (24). 93.0% of the modeled values lie within the dashed lines, which represent values with 2% of the correct value; the model-actual correlation coefficient is $r = 0.829$.

Although we were unable to model the remaining variability of f_L in terms of the IOPs or other parameters, this may be of little importance in predicting f_L itself, because f_L is always near one. However, the variability in f_L determines the variability in the fractional forward scattering coefficient $B_f = b_f(1 - f_L)$. Small fractional errors in f_L can cause large fractional errors in B_f. Figure 5 shows the resulting scatter plot for B_f, computed using the exact values of b_f as found in the database. Although 93.0% of the f_L values are within 2% of their correct value, only 5.4% of the B_f values are within 2% of the correct value; 58.1% of the B_f are within 20% of correct. However, a percentage error criterion may be misleading for B_f because of the cluster of points near zero, where small absolute errors can be large fractional errors. The dotted lines in Fig. 5 thus show absolute errors of ±0.02 m^{-1}; 94.5% of the B_f have errors smaller than this. The model-actual correlation coefficient is $r = 0.966$.

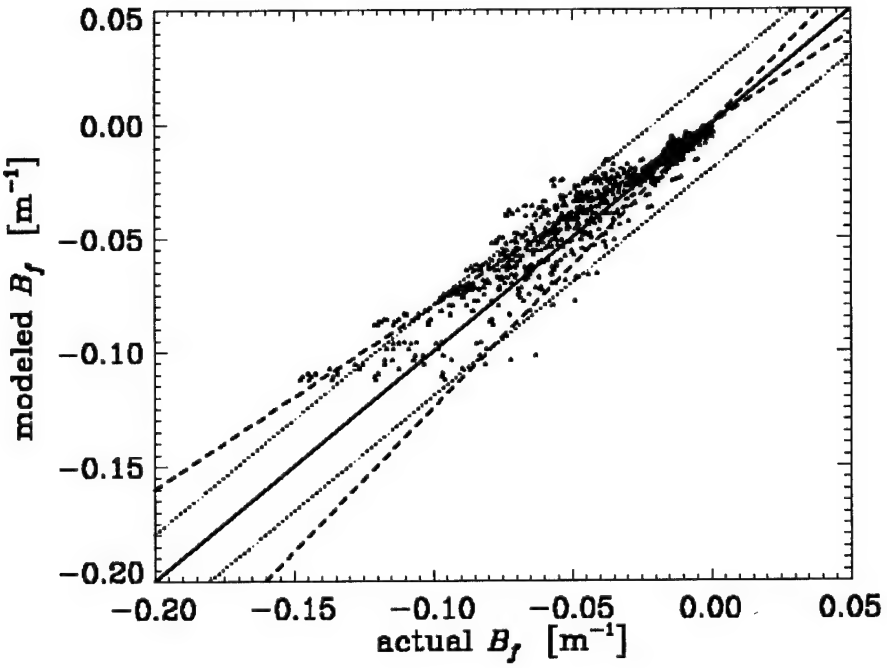

Fig. 5. Comparison of modeled and actual B_f values, computed using the f_L model of Eq. (26). The dashed lines are 20% error bounds; the dotted lines are ±0.02 m^{-1} error bounds.

4.5. The Model for k

The SSA again suggests a functional form for the $k(\theta,\varphi,z=0)$ model. Differentiating the SSA upwelling radiance of Eq. (25) gives

$$k(\theta,\varphi,0) = \left[-\frac{1}{L_u(z)} \frac{dL_u(z)}{dz} \right]_{z=0} \approx \frac{c}{\cos(\theta_s)}.$$

Although k is strongly correlated with a ($r = 0.99$), it is not strongly correlated with c ($r = 0.56$). At the level of the quasi-single-scattering approximation (QSSA), which often works well for upwelling radiances, $c \approx a + b_b$, in which case $k \approx (a + b_b)/\cos(\theta_s)$. This suggested that we first try to model k with the functional form

$$\hat{k} = \frac{\alpha_1 a + \alpha_2 b_b}{\cos(\theta_s)}. \tag{27}$$

When Eq. (27) was used to fit the points in the remote sensing data set, the points separated into distinct groups for $\theta_s \geq 60°$ and for $\theta_s < 60°$. We then plotted k and the residual error in k as functions of θ_s, which suggested that an additive $\sin(\theta_s)$ term would represent the θ_s dependence better than the $1/\cos(\theta_s)$ factor in Eq. (27). This then gave the final k model:

$$\hat{k} = \alpha_1 a + \alpha_2 b_b + \alpha_3 \sin(\theta_s). \tag{28}$$

The best-fit parameters are $\alpha_1 = 1.0896$, $\alpha_2 = -0.5931$, and $\alpha_3 = 0.0492$ (for a, b_b, and k in inverse meters). [Note that although θ_s in Eq. (28) refers to the polar angle of the solar beam in water, we can use the in-air solar zenith angle for θ_s, because the index-of-refraction factor that converts $\sin(\theta_s$ in air) to $\sin(\theta_s$ in water) is incorporated into α_3.] The points still separate somewhat by $\theta_s \geq 60°$ and for $\theta_s < 60°$, but not as much as for Eq. (27). Although Eq. (28) has lost some of its intuitive, first-order physics, namely the $1/\cos(\theta_s)$ factor in Eq. (27), the final model does a better job of predicting k, which of course is influenced by multiple scattering and other effects not included in the SSA. Figure 6 shows the scatter plot for the k model. Because of small differences near $k = 0$, only 76.8% of the points are within 20% of the correct value. However, 93.6% of the points lie within an absolute error of ± 0.05 m^{-1}. The model-actual correlation coefficient is $r = 0.993$.

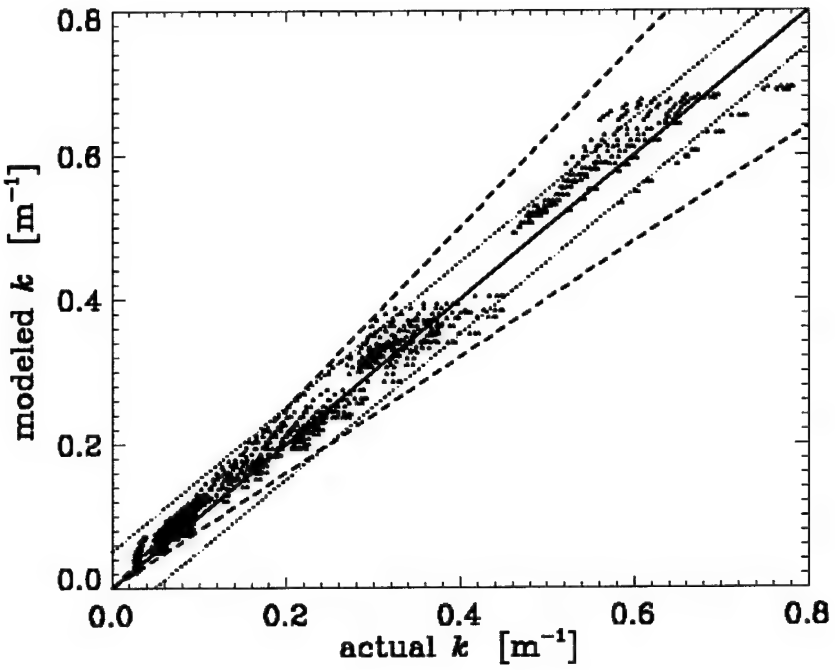

Fig. 6. The k model of Eq. (28). The dashed lines are the 20% error bounds, and the dotted lines are ± 0.05 m^{-1} error bounds.

4.6. The Model for R_μ

A first-order model for $R_\mu = \bar{\mu}_d(\text{in air}) / \bar{\mu}_d(\text{in water at } z=0)$ can be obtained simply by using Snell's law to refract the direct solar beam through a level water surface. The result is

$$R_\mu = \alpha_1 \frac{\cos\theta_s}{\cos\left[\sin^{-1}\left(\frac{\sin\theta_s}{n}\right)\right]} = \alpha_1 \Theta(\theta_s), \tag{29}$$

where $n = 1.34$ is the index of refraction of water. The ratio R_μ is independent of the viewing direction because the mean cosines are computed from integrals over direction of the radiance distribution; there are consequently many fewer distinct points in the data set. When Eq. (29) is applied to the RS data set, the best-fit value of α_1 is 0.869. Figure 7 shows the results of this model applied to all points in the RS data set. The six groups of points correspond to the six solar angles in the data set: $\theta_s = 0$, 10, 20, 30, 40, and 60 degrees. 85.7% of the points lie within 5% of the correct value, as shown by the dashed lines. The correlation coefficient is $r = 0.964$.

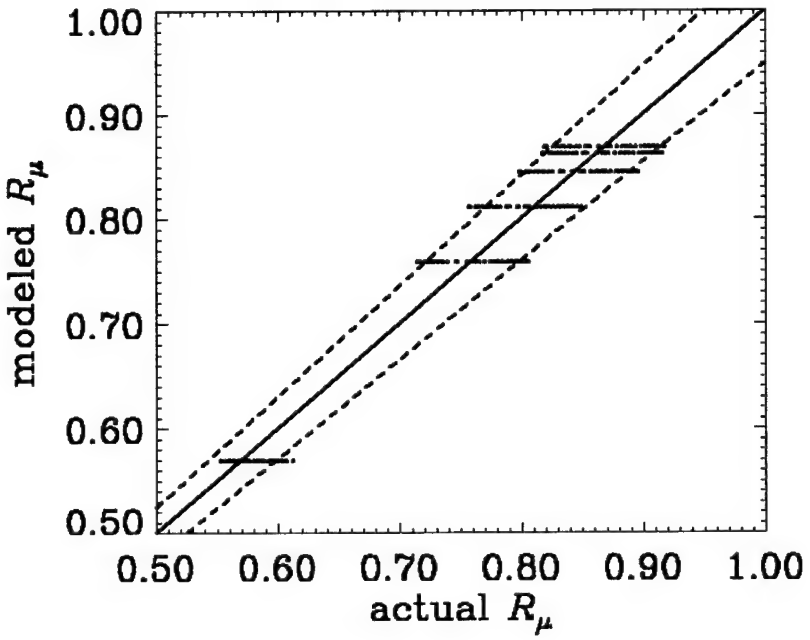

Fig. 7. The model of Eq. (29) applied to the RS data set. The dashed lines are 5% error bounds.

5. Discussion

We now have developed models that predict the shape factors and related quantities with varying degrees of certainty. The question next arises as to how well we can predict the remotely sensed reflectance RSR_a using these models in Eq. (9). Figure 8 gives the answer: 68.1% of the RSR_a predictions fall within 10% of the correct values, and 95.7% fall within 20% of correct (shown by the dashed lines in Fig. 8); 85.6% of the predictions are within ± 0.0005 sr^{-1} of the correct value. The model-actual correlation coefficient is $r = 0.983$.

We have already noted that inversion of the shape factor form of the RTE is exact from the standpoint of radiative transfer theory and that the uncertainties in the retrieved IOPs are due only to the accuracy of the IOP models [Hoge and Lyon 1996; Hoge et al. 1999a; Hoge et al., 1999b] and to the models for the shape factors and related quantities. The IOP models are fairly mature compared to the preliminary shape factor models presented here.

To understand how the remaining errors in the shape factor models, and in our ability to predict RSR_a, affects the accuracy of the retrieved IOPs, it is necessary to study performance of the iterative inversion algorithm outlined above via its application to both synthetic and actual data sets. The overall inversion is investigated first in the controlled environment of Hydrolight-generated synthetic RSR_a data, for which the correct IOP values are known from the input to Hydrolight. The inversion is then applied to actual RSR_a field data, for which the field measurements of the retrieved IOPs are themselves subject to experimental errors. Those evaluations of the overall inversion algorithm are the subject of the companion paper [Hoge et al., 2002].

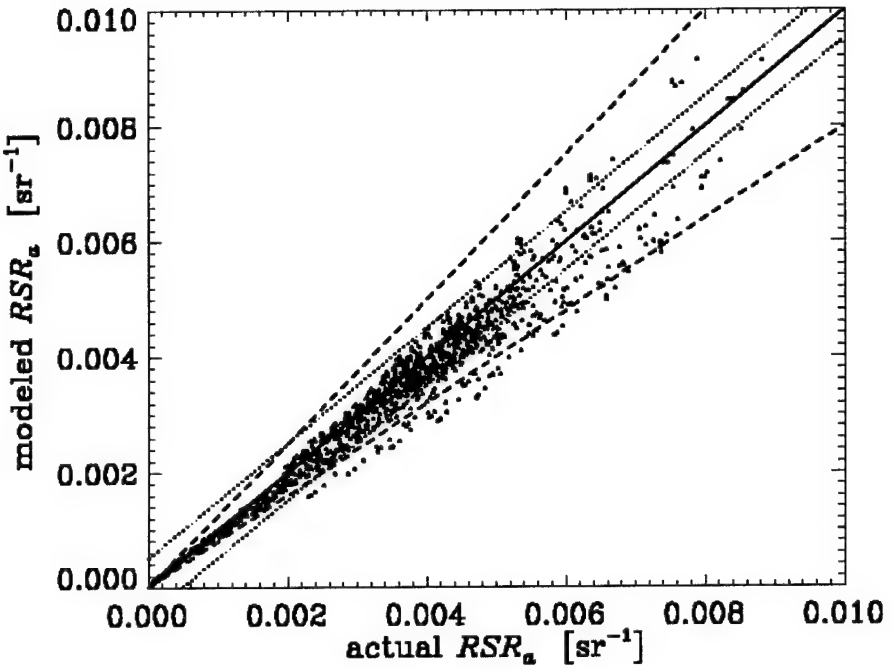

Fig. 8. RSR_a as modeled by Eq. (9) using the four shape factor models. The dashed lines are 20% error bounds; the dotted lines are ±0.0005 sr^{-1}.

Appendix A. Uncertainties in the IOP State Vector p

Sensitivity of **p** to Perturbations in **D**

Perturbations within **D** arise, for example, from the water-leaving radiances, scalar irradiances, backscattering shape factor, and from the IOP models. Similarly, uncertainties in **h** arise from the radiances, irradiances, hydrospheric constants (or IOP constants a_w and b_{bw}) for sea water, as well as f_b, $dL_u(\lambda_i)/dz$, $b_f(\lambda_i)$, $f_L(\lambda_i)$, and $cos\ \theta$. Relative to **h**, the data-model matrix, **D,** plays the major role in the propagation of errors into **p** since $\| \mathbf{p} - \mathbf{p}' \| / \|\mathbf{p}\| \leq \kappa(\mathbf{D}) (\| \Delta \| / \|\mathbf{D}\| + \| \delta \| / \|\mathbf{h}\|)$ where $\kappa(\mathbf{D}) = \|\mathbf{D}\| \|\mathbf{D}^{-1}\|$ [Ortega 1990; Hoge and Lyon 1996]. The latter expression is the condition number of **D**, and Δ and δ represent uncertainty or perturbation of **D** and **h** respectively. $\mathbf{p}'$ is the perturbed solution of **p**. The first expression simply states that to first order the relative error in **p** can be $\kappa(\mathbf{D})$ times the relative error in **D** and **h**. Thus, the propagation into **p** of the relative errors of both **D** and **h** is governed by the condition number of **D**. For any norm, $1 \leq \kappa(\mathbf{D}) \leq \infty$. For the limiting cases: $\kappa(\mathbf{D}) = 1$, **D** is said to be perfectly conditioned while for $\kappa(\mathbf{D}) = \infty$, **D** is singular. For intermediate values of $\kappa(\mathbf{D})$ the interpretation of the condition number is very subjective and must be evaluated separately. For "large" $\kappa(\mathbf{D})$ the **D** matrix is said to be ill-conditioned and large errors may be found in **p**. For "small" $\kappa(\mathbf{D})$ the **D** matrix is said to be well-conditioned and smaller errors may be found in **p**. Of the five components, only f_b occurs in **D** (via V) and therefore provides the strongest influence on the IOP retrieval errors. This is in agreement with Zaneveld [1995] who concluded that f_b is most critical since the in-water remotely sensed reflectance (see equation 1) is directly proportional to it. It is for this reason that RTE component model developments should probably focus on f_b. If other RTE components such as D_L (or dL_u/dz) and/or B_f are solved-for , then they too will appear in the **D** matrix and thereby further increase the errors in **p**. In part, the additional uncertainty in **p** will be due to D_L and/or B_f model errors. Also, in general the condition number increases as the number of unknowns increases [McCormick 1992] contributing to additional uncertainty in **p**.

Sensitivity of **p** to Perturbations in **h**

While the condition of **D** is most important in determining the errors in the IOP state vector **p**, the error propagation equation, $\| \mathbf{p} - \mathbf{p}' \| / \|\mathbf{p}\| \leq \|\mathbf{D}\| \|\mathbf{D}^{-1}\| (\| \Delta \| / \|\mathbf{D}\| + \| \delta \| / \|\mathbf{h}\|)$ shows that uncertainties in **h** also propagate into **p**.

Notation

a	total absorption coefficient, $a_t + a_w$, (m^{-1}); denotes "in air" when used as a subscript
a_d	absorption coefficient of CDOM and detritus (m^{-1})
a_{ph}	absorption coefficient of phytoplankton (m^{-1})
a_t	total constituent absorption coefficient, $a_t = a_{ph} + a_d$ (m^{-1})
a_w	absorption coefficient of water (m^{-1})
b	total scattering coefficient (m^{-1})
b_b	total backscattering coefficient, $b_b = b_{bw} + b_{bt}$ (m^{-1})
b_f	total forward scattering coefficient (m^{-1})
b_{bt}	total constituent backscattering (TCB) coefficient (m^{-1})
b_{bw}	backscattering coefficient of seawater (m^{-1})
B_f	fractional forward scattering coefficient, defined by Eq. (9) (m^{-1})
c	beam attenuation coefficient, $c = a + b$ (m^{-1})
CDOM	chromophoric dissolved organic matter
D	data and model matrix
det**D**	determinant of **D**
D_L	radiance derivative term, defined by Eq. (8) (m^{-1})
$E_{od}(z)$	downwelling scalar irradiance, in water (W m^{-2} nm^{-1})
E_{oda}	downwelling scalar irradiance, in air, just above sea surface, (W m^{-2} nm^{-1})
$E_d(z)$	downwelling plane irradiance, in water (W m^{-2} nm^{-1})
E_{da}	downwelling plane irradiance, in air (W m^{-2} nm^{-1})
$E_u(z)$	upwelling plane irradiance, in water (W m^{-2} nm^{-1})
E_{ua}	upwelling plane irradiance, in air (W m^{-2})
F_{ik}	modeling function
f_b	backscattering shape factor, dimensionless
$\hat{f}_b$	estimated backscattering shape factor, dimensionless
f_L	radiance shape factor, dimensionless
$\hat{f}_L$	estimated radiance shape factor, dimensionless.
$\overline{f_L}$	average of f_L values having θ_s in remote sensing data set
g	phytoplankton Gaussian model spectral width parameter (nm)
h	vector of hydrospheric constants, shape factors, radiance attenuation coef., (m^{-1})
IOP	inherent optical property
K_{Lu}	diffuse attenuation coefficient for upwelling radiance, $K_{Lu} = -d[\log L_u(z,\theta,\varphi)]/dz$
L_u	upwelling radiance, below sea surface (W m^{-2} sr^{-1} nm^{-1})
L_{ua}	upwelling radiance, in air, just above sea surface (W m^{-2} sr^{-1} nm^{-1})

M	$[(t\ \bar{t})/[(1-rR)n_w^2] \approx 0.529$ for nominal sea conditions, dimensionless.
n	total constituent backscattering coefficient spectral model exponent, as used in Eq. (14), dimensionless.
n_w	index of refraction of sea water, dimensionless.
P_k	modeling parameter
$\boldsymbol{p}$	oceanic state vector of retrieved IOPs, m^{-1}
r	water-to-air surface reflectance for plane irradiance, dimensionless
R	plane irradiance reflectance, in water, $E_u(z)/E_d(z)$, dimensionless
R_μ	ratio of air-to-water mean cosines for downwelling irradiance
RSR	remotely sensed reflectance, in-water, $L_u(\theta,\varphi,z)/E_{od}(z)$, (sr^{-1})
RSR_a	remotely sensed reflectance, in air, $L_{ua}(\theta,\varphi)/E_{oda} = \bar{\mu}_{da} R_{rs}$ (sr^{-1})
R_{rs}	remote sensing reflectance, in air, $L_{ua}(\theta,\varphi)/E_{da}$, (sr^{-1})
RTE	Radiative Transfer Equation
S	spectral slope within the a_d model for CDOM/detritus, (nm^{-1})
t	water-to-air radiance transmittance, dimensionless
$\bar{t}$	water-to-air plane irradiance transmittance, dimensionless
TCA	total constituent absorption, a_t , (m^{-1})
TCB	total constituent backscattering, b_{bt} , (m^{-1})
V	backscattering enhancement factor, defined by Eq. (12), dimensionless
X_i	shape factors and related quantities; defined in Table 1 for i = 1,2,...6.
z	depth, (m)
α_i	model fitting parameters, see tables for numerical values
β	volume scattering function
γ_i	model fitting parameters, see tables for numerical values
λ	wavelength, (nm)
λ_b	reference λ for total constituent backscattering (TCB) coefficient model, (nm)
λ_d	reference wavelength for CDOM/detritus absorption coefficient model, (nm)
λ_g	peak wavelength for Gaussian phytoplankton absorption coefficient model, (nm)
λ_L	peak wavelength for Gaussian model for depth derivative of radiance, (nm)
λ_i	wavelength of observational bands, i= 1, 2, 3, ..., (nm)
$\bar{\mu}_d$	average cosine for downwelling irradiance, in water, dimensionless.
$\bar{\mu}_{da}$	average cosine for downwelling irradiance, in air, dimensionless.
φ	azimuth angle, radians; subscripts v, s denote solar, viewing
θ	polar zenith angle in-water, radians; subscripts v, s, a denotes solar, viewing, in-air
ξ	included angle, solar-to-viewing direction
ω_o	single-scattering albedo

Acknowledgements

The continued support and encouragement of NASA Headquarters Ocean Biology Program is gratefully acknowledged. Authors C.D.M. and L.K.S. were supported by the Environmental Optics Program of the Office of Naval Research under contract no. N-00014-01-M-0268.

References

Davis, C. O., J. Bowles, R. A. Leathers, D. Korwan, T. V. Downes, W. A. nyder, J. J. Rhea, W. Chen, J. Fisher, W. P. Bissett, and R. A. Reisse, Ocean PHILLS hyperspectral imager: design, characterization, and calibration, *Optics Express, 10,* 210-221, 2002.

Gordon, H. R., Modeling and simulating radiative transfer in the ocean. Chapter 1 in *Ocean Optics* by R. W. Spinrad, K. L. Carder, and M. J. Perry, Oxford, 1994.

Gordon, H.R., O.B. Brown, R.H. Evans, J.W. Brown, R.C. Smith, K.S. Baker, and D.K. Clark, A semianalytic radiance model of ocean color, *J. Geophys. Res., 93*, 10,909-10,924, 1988.

Hoge, Frank E. and Paul E. Lyon, Satellite retrieval of inherent optical properties by linear matrix inversion of oceanic radiance models: An analysis of model and radiance measurement errors, *Jour. Geophys. Res., 101*, 16,631- 16,648, 1996.

Hoge, Frank E., C. Wayne Wright, Paul E. Lyon, Robert N. Swift, James K. Yungel, Satellite retrieval of inherent optical properties by inversion of an oceanic radiance model: A preliminary algorithm, *Applied Optics, 38*, 495-504, 1999a.

Hoge, F.E., C. Wayne Wright, Paul E. Lyon, Robert N. Swift, James K. Yungel
Satellite retrieval of the absorption coefficient of phytoplankton phycoerythrin pigment: Theory and feasibility status, *Appl. Opt., 38*, 7431-7441, 1999b.

Hoge, F. E., P. E. Lyon, C. D. Mobley, and L. K. Sundman, Inversion of the radiative transfer equation via shape factor models. Part II: Application. In preparation for submission to *J. Geophys. Res.*, 2002.

McCormick, N.J., Inverse radiative transfer problems: a review, *Nuclear Science and Engineering, 112*, 185-198, 1992.

Mobley, C.D., *Light and Water, Radiative Transfer in Natural Waters*, Academic Press, New York, 1994.

Mobley, C. D., Hydrolight 4.2 Users' Guide, Sequoia Scientific, Inc., Redmond, WA, 88 pages, 2001a. See also www.sequoiasci.com.

Mobley, C. D., Hydrolight 4.2 Technical Documentation, Sequoia Scientific, Inc., Redmond, WA, 79 pages, 2001b.

Mobley, C. D., B. Gentili, H. R. Gordon, Z. Jin, G. W. Kattawar, A. Morel, P. Reinersman, K. Stamnes, and R. H. Stavn. Comparison of numerical models for computing underwater light fields, *Appl. Optics* 32(36), 7484-7504, 1993.

Morel, Andre and Bernard Gentili, Diffuse reflectance of oceanic waters. III. Implication of bidirectionality for the remote sensing problem, *Appl. Opt., 35*, 4850-4862, 1996.

O'Reilly, S. Maritorena, B. G. Mitchell, D. A. Siegel, K. L. Carder, S. A. Garver, M. Kahru, and C. McClain, Ocean color chlorophyll algorithms for SeaWiFS, J. Geophys. Res., 103 (C11), 24937-24953, 1998.

Ortega, James M., Numerical Analysis, *A Second Course*, Society for Industrial and Applied Mathematics, Philadelphia, 1990.

Pope, Robin M. and Edward S. Fry, Absorption spectrum (380-700nm) of pure water: II. Integrating cavity measurements, *Appl. Opt., 36*, 8710-8723, 1997.

Smith, R.C., and K.S. Baker, Optical properties of the clearest natural waters (200 - 800 nm), *Appl. Opt., 20*, 177-183, 1981.

Weideman, Alan D., Robert H. Stavn, J.R.V. Zaneveld, and M.R. Wilcox, Error in predicting hydrosol backscattering from remotely sensed reflectance, *Jour. Geophys. Res., 100*, 13,163 - 13,177, 1995.

Zaneveld, J. Ronald V., Remotely sensed reflectance and its dependance on vertical structure: a theoretical derivation, *Appl. Opt., 21, 4146-4150*, 1982.

Zaneveld, J. Ronald V., A theoretical derivation of the dependance of the remotely sensed reflectance of the ocean on the inherent optical properties, *J. Geophys. Res,. 100*, 13,135- 13,142, 1995.